

# From Retinex to Automatic Color Equalization: issues in developing a new algorithm for unsupervised color equalization

Alessandro Rizzi

Carlo Gatta

University of Milano

Department of Information Technology

Via Bramante, 65

26013 Crema, Italy

E-mail: rizzi@dti.unimi.it, gatta@dti.unimi.it

Daniele Marini

University of Milano

Department of Science Technology

Via Comelico, 39

20100 Milano, Italy

---

**Abstract.** We present a comparison between two color equalization algorithms: Retinex, the famous model due to Land and McCann, and Automatic Color Equalization (ACE), a new algorithm recently presented by the authors. These two algorithms share a common approach to color equalization, but different computational models. We introduce the two models focusing on differences and common points. An analysis of their computational characteristics illustrates the way the Retinex approach has influenced ACE structure, and which aspects of the first algorithm have been modified in the second one and how. Their interesting equalization properties, like lightness and color constancy, image dynamic stretching, global and local filtering, and data driven dequantization, are qualitatively and quantitatively presented and compared, together with their ability to mimic the human visual system. © 2004 SPIE and IS&T. [DOI: 10.1117/1.1635366]

---

## 1 Introduction

What our visual system perceives is not the color of an object, but the combination of its spectral reflectance with the illuminant's spectral characteristics. Consequently, from a photometric viewpoint, a yellow patch illuminated with a white light or a white patch illuminated with a yellow light can reflect the same spectral distribution. Changes in the illuminant should produce changes in the perceived image. However, the human visual system (HVS) steadily perceives a scene regardless of changes in the lighting conditions,<sup>1</sup> thanks to a perceptual mechanism called *color constancy*.

This mechanism is able to separate, with a certain tolerance, the reflectance from the illuminant in a perceived

signal. Thus, color constancy can be defined as the capability to isolate the object's reflectance from the illuminant's spectral composition, or alternatively, to recover the object's chromatic appearance without regard to the color of the light. These two definitions of color constancy may seem very similar, but they are not. Choosing one over the other can heavily influence the goal of a color constancy algorithm.

An algorithm that follows the first definition considers the color constancy phenomenon mainly from a physical viewpoint. In this case, color constancy results in a signal reconstruction problem. If the illuminant can be estimated, then the object's reflectance can be approximated. Since the spectral content of the original scene is lost and the available information is only a pixel value, usually the best results of this approach are obtained with a standard illuminant, or with an illuminant whose spectral content is known.

The second definition of color constancy mimics the perceptual mechanisms of HVS and leads to an approach in which color recovery is not necessarily perfect. In fact, while HVS stabilizes perception when there are illuminant variations, from another viewpoint, the perceptual mechanisms make the object's appearance dependent on the chromatic and spatial composition of the scene.<sup>2,3</sup>

A consequence of this fact is that the visual appearance of a scene cannot be explained with just a global approach; identical visual stimuli with different spatial distribution can result in different visual appearances. A classic example of this fact is a well-known visual configuration called simultaneous contrast, which arises, e.g., when a small gray square lays over a larger and saturated background color. In this case, what the observer perceives is not gray, but a hue

that tends toward the complementary color of the background.

The approach of Retinex, the model of HVS color perception due to Land and McCann,<sup>4</sup> is consistent with these considerations. It assumes that color sensation is based on the ratios of reflected light intensity in specific wavelength bands computed between adjacent areas of the image. For about 40 years, variants of the Retinex method have been implemented in software and hardware,<sup>5-17</sup> and now it shows a renewed research interest.<sup>18</sup>

Following this approach, we have developed an alternative digital image automatic enhancement algorithm called Automatic Color Equalization (ACE) that, as well as Retinex, is able to simulate HVS mechanisms, such as color constancy and lightness constancy. Our aim in developing ACE is to implement a system that emulates HVS adaptation properties, considering low-level principles like independent computation of chromatic channels,<sup>7</sup> lateral inhibition mechanisms,<sup>19</sup> global/local mechanisms,<sup>20</sup> white patch (WP),<sup>21</sup> and gray world (GW)<sup>22</sup> adapting mechanisms. In other words, ACE mimics the behavior of the HVS, reproducing its adaptation mechanisms in a qualitative way. To differentiate the real HVS process from its model, we use the word “adaptation” to indicate the biological adaptations made by the HVS in the real world, and the word “adjustment” to indicate the simplified adaptations of these algorithms in the digital image domain. In particular, the term *adaptation* refers more to a colorimetric notion than to the dark and light adaptation phenomena.<sup>23</sup>

The next section presents the Retinex and ACE computational models, and Sec. 3 illustrates their common aspects and how the Retinex approach has influenced ACE structure. Then, Sec. 4 analyzes the major filtering properties of the two algorithms, with qualitative and quantitative comparisons. Conclusions end the work.

## 2 Computational Models

### 2.1 Retinex

For an extensive and detailed description of the history and experiments of this famous model, we ask the reader to refer to Refs. 4, 7, 15, and 24–27. In this work, we simply recall the basic formula and the relative concepts to make the corresponding comparisons with the proposed algorithm ACE.

The Retinex theory assumes that human vision is based on three retinal-cortical systems, each independently processing the low, middle, and high frequencies of the visible spectrum. Each independent process forms a separate image, determining the relative lightness values of the various regions of a scene.<sup>25</sup> According to Land and McCann, the edges between adjacent areas of an image play a fundamental role in color perception. Therefore, the ratio of lightness between two areas has been chosen as a dimensionless property describing their relationship. If these two areas have lightnesses that are very different, the ratio is far from the unitary value, and it tends toward the value of 1, where the lightnesses tend to become equal. If the ratio is computed and averaged in many locations of the image, it discounts possible chromatic dominance, and its dimensionless character will equalize the overall lightness of the image.

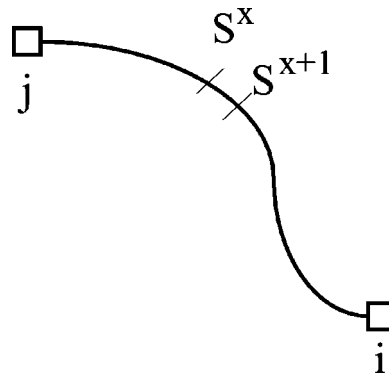


**Fig. 1** Along the path from point  $j$  to point  $i$ , the relative lightness is computed as the ratio between the visual responses at the generic points  $x$  and  $x+1$ .

The visual response  $S^x$  at the location  $x$  of the image is:

$$S_{R,G,B}^x = \int_{\lambda \in (400 \text{ nm}, 700 \text{ nm})} E(\lambda) R^x(\lambda) \rho_{R,G,B}(\lambda) d\lambda, \quad (1)$$

where  $x$  is a discrete spatial coordinate,  $E(\lambda)$  is the spectral power distribution of the illuminant light,  $R^x(\lambda)$  is the reflectance at the point  $x$ , and  $\rho_{R,G,B}(\lambda)$  is the spectral sensitivity of the photoreceptor's (retinal cones) pigment.

The relative lightness  $L_{R,G,B}^{i,j}$  at point  $x$ , along a random path in the image (see Fig. 1), for each channel  $RGB$ , is computed in the following way:

$$L_{R,G,B}^{i,j} = \sum_{x \in \text{path}} \delta \log \frac{S^{x+1}}{S^x}, \quad (2)$$

where

$$\delta = \begin{cases} 1 & \text{if } \left| \log \frac{S^{x+1}}{S^x} \right| > \text{threshold} \\ 0 & \text{if } \left| \log \frac{S^{x+1}}{S^x} \right| < \text{threshold} \end{cases} \quad (3)$$

Hence, the recalculated  $RGB$  intensity value for each point  $i$  is the mean value of relative lightnesses  $L_{R,G,B}^{i,j}$  computed over a number  $N$  of random paths, ending at point  $i$  (Fig. 2):

$$S_{R,G,B}^i = \frac{\sum_{k=1}^N L_{R,G,B}^{i,j_k}}{N}. \quad (4)$$

These computations must be executed separately for the three fundamental channels  $RGB$ .

This model depends on the number and randomness of the chosen paths, and on the threshold value that makes it possible to disregard low lightness ratios, which correspond to smooth changes in color due to nonuniform illumination.

The basic Retinex algorithm has a reset mechanism by means of which, during a path computation, if a lighter area is found, the cumulated relative lightness is forced to the

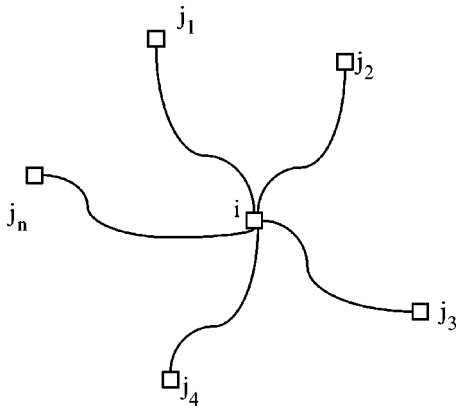


**Fig. 2** Example of random paths from random points ( $J_1 - J_n$ ) for the computation of the lightness value at point  $i$ .

unitary value, making the average computation restart from this area. The effect of the reset mechanism is to consider the lightest area of an image as a local reference value for white.

**2.2 ACE**

To approximate the visual appearance of a scene, we have developed a model, trying to simultaneously combine in a unique computation some of the mechanisms involved in human visual perception.<sup>28</sup> Within this model, every basic principle is considered as part of a unique adaptive behavior involving the contribution of each mechanism to the final result. Each adaptive mechanism has global and local effects as a consequence of a number of simple local operations across the image.

The algorithm has been implemented following the scheme shown in Fig. 3. The first stage accounts for chromatic spatial adjustment and models two important mechanisms: lateral inhibition and global/local adaptation. These two mechanisms form the basis of the appearance computation of each area in the image, taking into account their neighboring and dimensional relationship. Then, the second stage maximizes the image dynamic, normalizing the white at a global level and performing a global gray world behavior. This two-phase structure is a characteristic in a majority of the HVS computational models in the field of digital imaging.<sup>29,30</sup> In Fig. 3,  $I_c$  is the input image,  $R_c$  is an intermediate result, and  $O_c$  is the output image, while subscript  $c$  denotes the chromatic channels.

As well as Retinex, this algorithm requires no user supervision or *a priori* knowledge of the image acquiring

condition. This makes it suitable for use on uncalibrated images.<sup>31</sup>

**2.2.1 Chromatic/spatial adjustment**

In the first stage, the chromatic/spatial adjustment produces an output image  $R_c$ , in which every pixel is recomputed according to the image content.

The algorithm is mainly driven by two parameters, which are described later. In particular,  $r(\cdot)$  function influences the white patch behavior and the image contrast. The  $d(\cdot)$  function has been formally devised to include the concept of spatial influence; consequently, a change of its shape influences the ACE global/local effect.

In this phase, each pixel  $p$  of the output image  $R_c$  is computed separately for each channel  $c$  as follows:

$$R_c(p) = \sum_{j \in \text{Image}, j \neq p} \frac{r[I_c(p) - I_c(j)]}{d(p, j)}, \tag{5}$$

where  $I_c(p) - I_c(j)$  accounts for the lateral inhibition mechanism,  $d(\cdot)$  is a distance function that weights the amount of local or global contribution, and  $r(\cdot)$  is the function discussed later that accounts for the relative lightness appearance of the pixel. A preliminary comparison on  $d(\cdot)$  has shown that the Euclidean distance, or its approximations like *Manhattan*, give the best results.<sup>28</sup>

For each pixel in the image  $r(\cdot)$ , together with  $d(\cdot)$ , controls the relative pixel's influence, accounting for spatial channel lightness adjustment. They compute all of the single contributions of the image's content to each final pixel value in the output image. These two functions do not affect directly the final pixel saturation, since the formula inside the summation computes the influence of only one pixel, and to obtain the final pixel value, it must be calculated for all the pixels in the image. In other words, the final pixel value is the summation of nonlinear contributions that can have different signs due to the spatial pixel relationship. It is possible for a channel to be saturated, but this can only occur during the final stage of the process, the dynamic tone reproduction scaling, which we describe next.

The chosen set of  $r(\cdot)$  functions is shown in Fig. 4.

The  $r(\cdot)$  function slope variation acts as a contrast tuner. It can be seen in the  $r(\cdot)$  function comparison shown in Fig. 5. The higher the slope is, the higher the contrast. The  $r(\cdot)$  function slope parameter can vary from the unitary value to infinite (signum in Fig. 4).

In the basic formula in Eq. (5), no compensation is computed for the distance of the pixel from the picture margin.

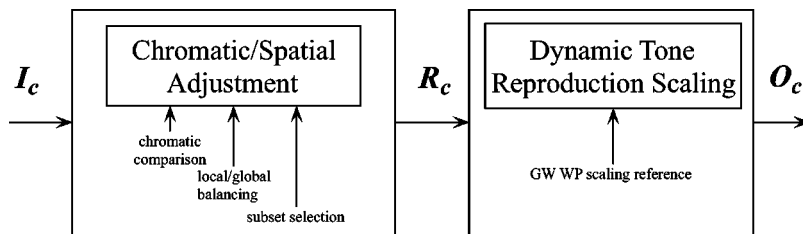


**Fig. 3** Basic ACE structure.

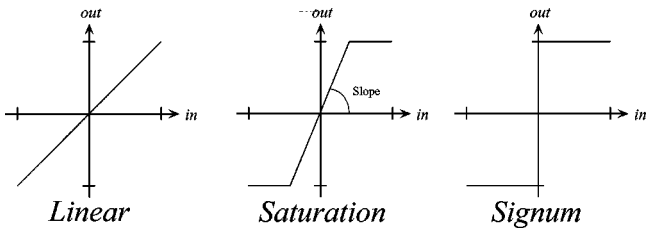


Fig. 4  $r(\cdot)$  function set.

If the pixel is near the margin, the number of pixels near it decrease significantly. These neighboring pixels give an important contribution, since the inverse of  $d(\cdot)$  has high values only around the pixel (see Fig. 6). Consequently, Eq. (5) has been modified with a normalization coefficient in the following way:

$$R_c(p) = \frac{\sum_{j \in \text{Image}, j \neq p} \frac{r[I_c(p) - I_c(j)]}{d(p, j)}}{\sum_{j \in \text{Image}, j \neq p} \frac{r_{\max}}{d(p, j)}}, \quad (6)$$

where  $r_{\max}$  is the maximum value of function  $r(\cdot)$  independently from the image content.

### 2.3 Dynamic Tone Reproduction Scaling

The output values in the intermediate pixel matrix  $R$ , which are real numbers, can range from  $min$  to  $max$ , where  $min$  and  $max$  are arbitrary values that depend on the content of the picture. Thus, for each chromatic channel, we have to map this range into the integer interval  $(0, 255)$  of the final output image  $O$ , choosing reference values to translate and scale this interval.

The proposed method linearly scales the values in  $R_c$  with the following formula:

$$O_c(p) = \text{round}[127.5 + s_c R_c(p)], \quad (7)$$

for each pixel  $p$ , where  $s_c$  is the slope of the segment  $[(0, 127.5), (M_c, 255)]$  computed by Eq. (8), with  $M_c = \max_p R_c(p)$ .

$$s_c = \frac{M_c - 0}{255 - 127.5} = \frac{M_c}{127.5}. \quad (8)$$

It uses  $M_c$  as a white reference and the zero value in  $R_c$  as an estimate for the medium gray reference point to compute the slope  $s_c$ . For this reason, the available dynamic could not be used in its entirety, and tones around the very dark values could be lost. Alternatively, some pixels in  $O_c$  can result in negative values. In this case, the values lower than zero are set to zero.

This method adds a global gray world adjustment in the final scaling. Thus the dynamic of the final image is always centered around the medium gray. According to the chosen reference point, alternative scaling methods can be devised to take into account nonlinearities typical of human luminance perception without changing ACE's two-phased structure.

### 3 From Retinex to ACE

The two algorithms share a common approach and several computational characteristics, but differ in many nontrivial details. Since we are interested in comparing the fundamental principles of the two approaches, the following qualitative comparisons consider only the basic algorithms, with no discussion on particular implementations or optimized versions.

An important common point is that in both the algorithms, the three chromatic channels are processed separately. Differences are described in the following subsections.

#### 3.1 Comparing Image Pixels: Ratio Versus Difference

While Retinex uses the ratio to compute the relative appearance of each pixel, ACE uses pixel subtraction. The real

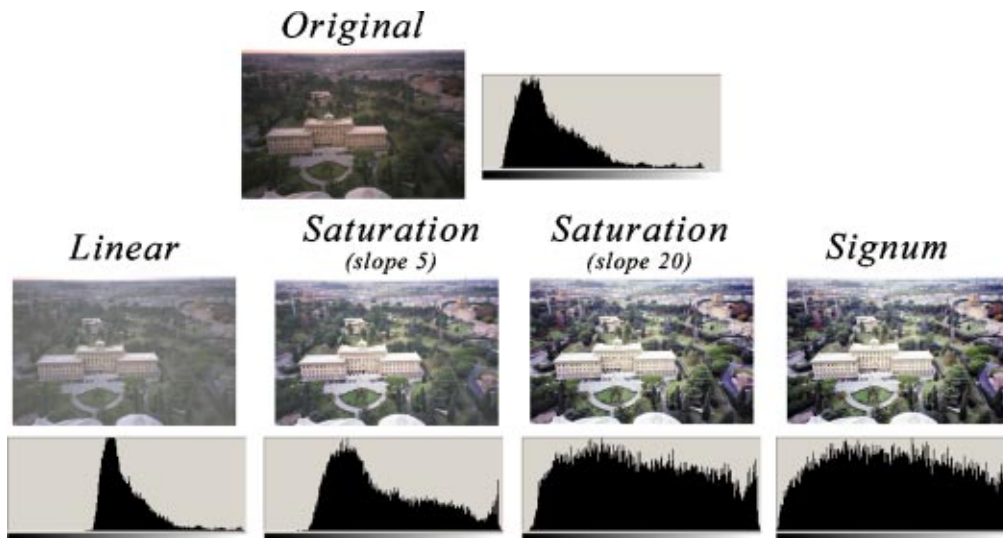


Fig. 5 Sample image filtered with different  $r(\cdot)$  functions (after the *dynamic tone reproduction scaling* stage).

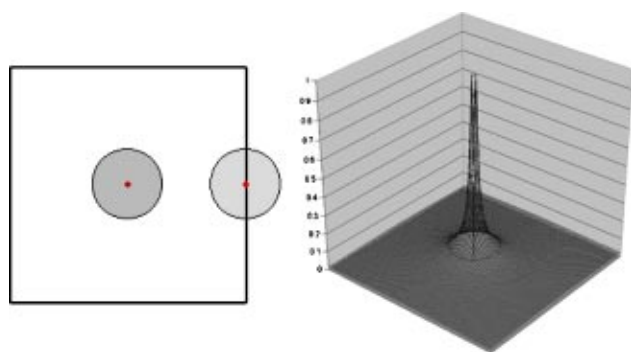


Fig. 6 Computational asymmetries due to the distance  $d(\cdot)$  near the image margins.

difference between the two is not based on this fact (in a logarithmic space, the ratio becomes a difference), but on the fact that ACE's subtractions are distorted by the amplifying function  $r(\cdot)$ . This nonlinearity is responsible for the final contrast. Eliminating such distortion leads to unsatisfactory results, as can be seen in the left of Fig. 5.

### 3.2 Nonlinearity in Perception: Reset Versus Amplifying Function

In the Retinex model, the reset mechanism is devised to perform a sort of "search for the channel maximum," that can be seen as a kind of local white patch behavior. The locality of this effect, in the basic algorithm, depends on the number and the randomness of the paths, in other implementations on the hierarchy of the decomposition,<sup>7</sup> or on the shape of the filtering function.<sup>5</sup> The reset introduces a nonlinearity that follows the nonlinearity of perception, and is one of the major characteristics of this family of algorithms and also the basis of their local effect.

This nonlinearity is maintained in ACE by the amplifying function  $r(\cdot)$  that emphasizes the single pixel difference. It enhances the relative influence of brighter and dimmer zones around the pixel being computed, weighted by distance  $d(\cdot)$ . This mechanism, repeated for every pixel, expands and compresses the dynamic range in different areas of the image, driven by the local image content. As a final result, this pixel difference enhancement acts as a sort of local maximum referencing, similar to the Retinex reset.

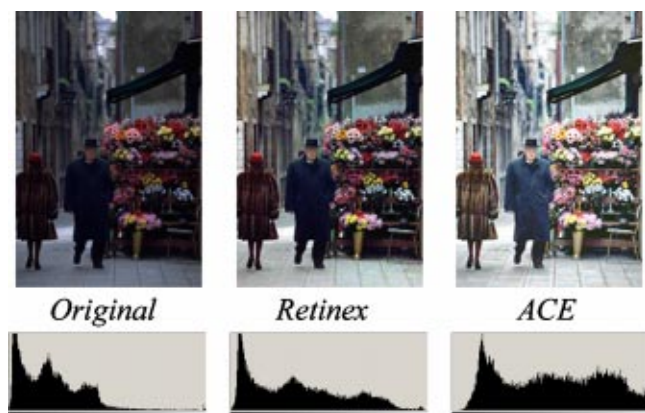


Fig. 7 Lightness constancy effect on a low-key image.

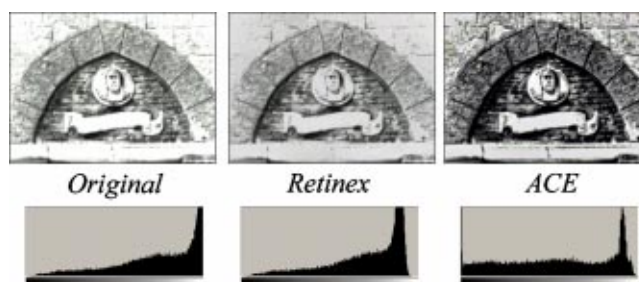


Fig. 8 Lightness constancy effect on a high-key image.

### 3.3 Exploring the Image: Random Paths Versus Global/Local Weighting Distance

The various Retinex implementations differ in the way they explore the image. McCann's Retinex compares each pixel with its eight-neighbors in a multilevel framework.<sup>7</sup> Our implementation uses Brownian random paths,<sup>34</sup> inspired by Zeki's studies about receptive field centroid distribution.<sup>35</sup> NASA Retinex uses a convolution with a predefined function that includes the concept of global/local filtering.

With a similar approach in considering locality, ACE uses a distance function weighting the contribution given to a pixel by comparing it with other pixels in the image. The shape of this weighting function can be seen in the right of Fig. 6.

Even if in different ways, the pixel recomputation across the image allows these algorithms to simulate several local chromatic perceptual effects, e.g., the simultaneous contrast or the Cornsweet effect.<sup>28,34,36</sup>

### 3.4 Second Stage: Dynamic Tone Reproduction Scaling

This second and final stage prepares the computed image for visualization. Based on ratios, Retinex produces output values for each chromatic channel in the range [0-1]. These values are scaled into the available dynamic range only at the end of computation. Due to the reset mechanism that

Table 1 Lightness and dynamic data of the two images of Figs. 7 and 8.

Dark image	Original	Retinex	ACE
Mean	49.87	84.44	128.64
Histogram flatness	38779	20347	12656
% used dynamic	91.41%	98.44%	96.09%
% unused black	0%	0.39%	3.51%
% unused white	0%	1.17%	0%
Light image	Original	Retinex	ACE
Mean	194.86	181.04	131.88
Histogram flatness	48669	52357	22442
% used dynamic	98.82%	95.31%	99.61%
% unused black	1.17%	1.17%	0%
% unused white	0%	3.51%	0.39%



**Fig. 9** Visual comparison of different global and local equalization algorithms on the synthetic image under illuminant A.

searches the white, more precise results are usually obtained in recovering high-key colors. Precision can decrease with very dark tones.<sup>37</sup>

Also, ACE maps the output of its first phase, held in the intermediate pixels matrix  $R$ , into the final output image  $O$ . This second phase is not a simple linear scaling. The higher  $R$  value is chosen as white reference, and the zero of  $R$  as the medium gray value, for each channel. For this reason, the available dynamic could not be used entirely, and tones around the very dark values could be lost or distorted. Therefore, the blacks are not balanced with respect to the whites, preferring instead a global balance between gray world and white patch. This causes ACE to behave like Retinex for dark tone values.

#### 4 Digital Equalization Properties

In this section, we present an overview of the more significant Retinex and ACE filtering properties, with quantitative and/or qualitative measures.

The Retinex implementation used for this comparison is the Brownian paths.<sup>34</sup> It has been proven that choosing one version over another does not significantly change the final result.<sup>38</sup> Except where noted, the parameters used for Retinex are: paths=20, threshold=0.05, max Brownian displacement=40 pixels, and Brownian levels=3.

Regarding ACE, except where noted, the parameters are: saturation function with slope 20 as  $r(\cdot)$ , and Euclidean distance as  $d(\cdot)$ .

If not differently specified, all the example images are uncalibrated. Consequently, all the following tests are not

**Table 2** Mean  $\Delta E$  on original synthetic images.

Original	A	B	C	D65	Hg	Mix
A	0					
B	36.12	0				
C	52.56	17.06	0			
D65	48.56	12.51	6.45	0		
Hg	46.1	18.42	21.05	19.15	0	
Mix	27.1	9.52	25.76	21.55	24.49	0

**Table 3** Mean  $\Delta E$  on Retinex filtered synthetic images.

Retinex	A	B	C	D65	Hg	Mix
A	0					
B	11.74	0				
C	15.41	7.81	0			
D65	14.37	7.55	5.78	0		
Hg	18.68	13.47	12.48	12.98	0	
Mix	11.77	9.75	11.21	9.87	15.52	0

devised to produce quantitative measures of HVS simulation capabilities. However, qualitative HVS behavior can be very useful in digital image processing, as presented in the following sections, and as confirmed by various applications of Retinex in the field of digital imaging.

#### 4.1 Lightness Constancy and Dynamic Modification

One of the main effects of an equalization algorithm is the image's mean lightness adjustment. Retinex, like most of the color correction algorithms that search for the white, tends to increase the overall lightness of the image if its mean lightness is below the medium gray, but does not change it significantly if its mean is over the medium value. On the contrary, ACE, due to its gray world behavior component, is able to modify the image's mean lightness in both directions, according to its original value. This difference has been eliminated in some recent Retinex implementations.<sup>10</sup>

In Figs. 7 and 8, two examples of lightness equalization are shown. In the first image that is slightly underexposed (low key), both Retinex and ACE increase the mean lightness, while in the second one that is overexposed (high key), only ACE reduces the mean lightness. Since Retinex is a WP algorithm, to equalize toward the dark tones, it should be combined with an alternative mechanism, like GW.

In the example of Fig. 7, the effect of the two algorithms on the image dynamic is very similar. It can be verified qualitatively from the image histograms and quantitatively from the values presented in Table 1.

In this table, *histogram flatness* is the  $L1$  distance between the image histogram and a flat histogram on the same image size, the percent *used dynamic* is the percentage of the used values in the available dynamic range, and the percent *unused black* and percent *unused white* are the percentage of contiguous unused values in the lower and upper

**Table 4** Mean  $\Delta E$  on ACE filtered synthetic images.

ACE	A	B	C	D65	Hg	Mix
A	0					
B	6.19	0				
C	7.22	1.81	0			
D65	6.94	1.68	1.33	0		
Hg	8.48	5.05	5	5.09	0	
Mix	8.74	8.08	8.63	8.46	10.34	0

part of the histogram, respectively. Histogram flatness values are not normalized to the image size, since we are interested in comparing differences of this value on the same image, before and after the two filtering: lower values correspond to flatter histograms.

Note from the values in Table 1 that ACE moves the lightness mean toward medium gray and increases the percentage of used dynamic and flatness of the histogram. Retinex, in the low-key image, has a smaller effect on the mean lightness, but a larger increment of used dynamic. On the contrary, on the high-key image its effect is almost null.

#### 4.2 Color Constancy

To measure the algorithms ability to perform *color constancy*, we have computed the mean  $\Delta E^1$  distance across all the corresponding pixels between two images of the same size:

$$\Delta E_{\text{mean}} = \frac{\sum_{p \in \text{Image}} \Delta E[I_1(p), I_2(p)]}{\text{size } x \cdot \text{size } y},$$

where  $I_1$  and  $I_2$  are the images to be compared, and size  $x$  and size  $y$  are the image size in pixels.

This measure allows ideal color constancy. A null  $\Delta E$  value indicates a perfect discount of the illuminant, and consequently an absolute recovery of the object's corresponding colors. Such a separation does not occur under real conditions: HVS performs a significant, but incomplete, adaptation.<sup>24</sup> Thus, the significance of this measure comes from its variation before and after the adjustment. Consequently, no absolute meaning can be assigned to its numerical value.

To test this feature, we have used a set of six synthetic images generated by a photometric ray tracer program from the same 3-D scene using six different lighting conditions. The six synthetic images were generated with a photometric ray-tracing algorithm<sup>39</sup> from a 3-D livingroom model. Spectral radiance for each pixel has been computed from a synthetic model of virtual scene. The scene is characterized in terms of geometry of objects, spectral reflectance of surfaces, and spectral power distribution of illuminants.  $XYZ$  tristimulus values of each pixel are computed from the radiance using the CIE31 color matching function, and then are converted to  $sRGB$  color space. The light sources used were the standard CIE illuminant A, B, C, D65, and a Hg lamp; the latter image was obtained using a mix of these illuminants.

A visual comparison of different global and local equalization algorithms on the synthetic image under illuminant A is shown in Fig. 9. Note that *histogram equalization* and *white patch* are not able to eliminate the color cast; *gray world* seems able to accomplish the task, but the result is visually poor. By contrast, both Retinex and ACE results are satisfactory.

We have measured the mean  $\Delta E$  chromatic distance for any two illuminants on the original (Table 2), on the Retinex (Table 3), and on the ACE filtered images (Table 4).

A visual comparison of Retinex and ACE filtering on the entire image set is shown in Fig. 10. Note that the chromatic dominant of the illuminant is always significantly

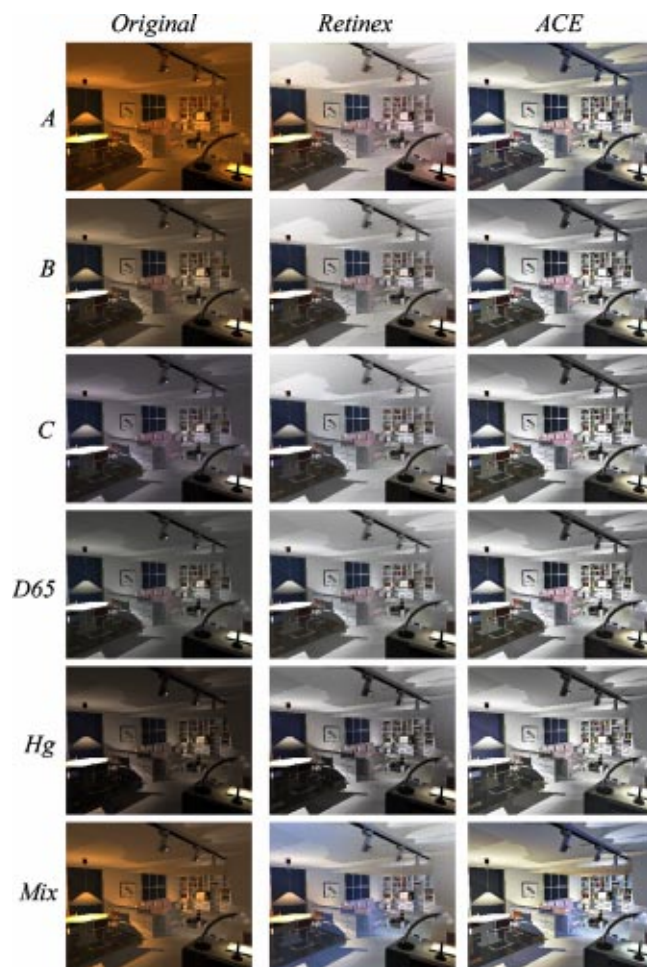


Fig. 10 Visual comparison of Retinex and ACE filtering on synthetic images.

reduced with filtering. In the image with more than one illuminant, both Retinex and ACE leave some local color bleeds. This result is consistent with human behavior, where if different illuminants are present in the field of view, color constancy fails, and we can notice easily the illuminant color.

A quantitative result comparison of the global and local equalization algorithms shown in Fig. 9 is visible in Fig. 11. The mean  $\Delta E$  distance of the original images is normalized to 100 to measure the other distances in terms of percentage. In the worst case, *histogram equalization*, this distance is increased by a factor of 10%; Retinex decrease

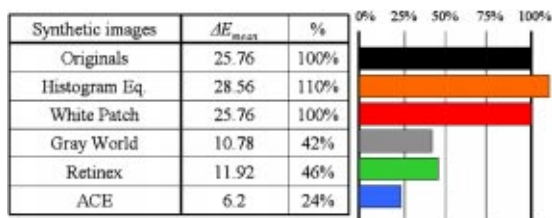


Fig. 11 Quantitative result comparison among different equalization algorithms.

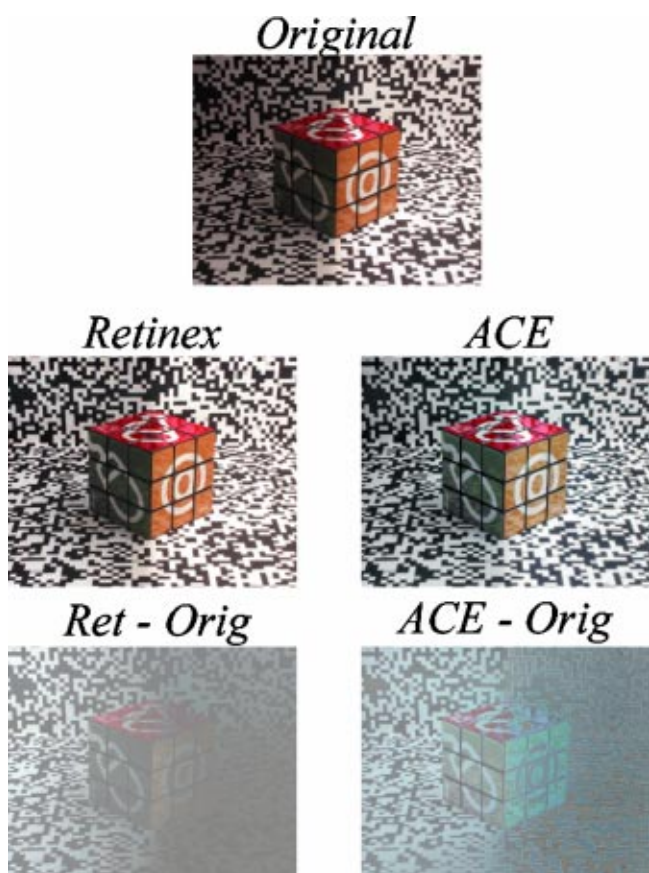


Fig. 12 Retinex and ACE local filtering effect.

it to 46%, while ACE performs better with a reduction to 24%.

### 4.3 Global and Local Filtering Effect

To test the locality of the two algorithms, we have used images from a new database (DB), realized by the authors, devised for color constancy algorithm comparison.<sup>40</sup>

Images in this DB have been captured under different illuminants, using two illumination patterns: a diffuse lighting and the same lighting divided by a shadow due to partial light occlusion. The presence of different lightness levels in the same image allows for the testing of local effects in color correction.

One of the images chosen from this DB is shown in Fig. 12, together with the Retinex and ACE outputs, including the respective image differences from the original. Both Retinex and ACE simultaneously perform global and local filtering, as shown through the analysis of the image differences, visualized around the medium gray in the figure.

Table 5 Mean lightness of the left and right parts of the images in Fig. 12.

Mean lightness	Original	Retinex	ACE
Left	61.74	100.18	102.03
Right	147.93	159.35	154.02
Right - left	86.19	59.17	51.99

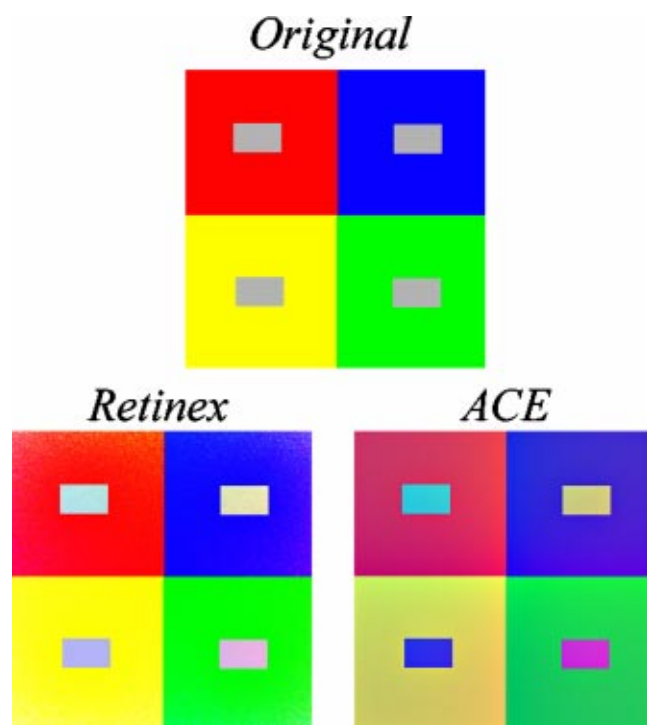


Fig. 13 Simultaneous contrast visual configuration and the relative Retinex and ACE filtering.

Again, the effect of the two algorithms is very similar, eliminating the shadow. A quantitative comparison of the filtering effects is visible in Table 5, where the mean lightness of the left and right parts of the images in Fig. 12 are presented. Another example of local filtering is presented in Fig. 13.

### 4.4 Data-Driven Color Dequantization

Using Retinex or ACE to filter an image with a limited color palette results in a data-driven color dequantization. This interesting property derives from their local behavior, according to which all of the pixels are recomputed in re-

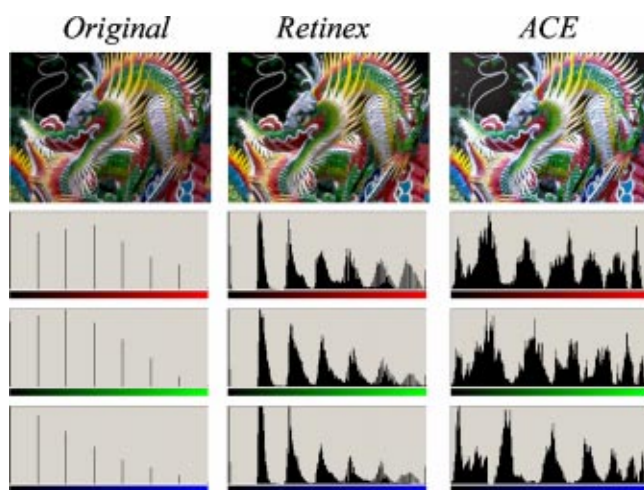


Fig. 14 Retinex and ACE color dequantization.

**Table 6** Percentage of used image dynamic before and after filtering.

	Quantized	Retinex	ACE
% used dynamic	41.4%	97.65%	99.21%

lation to the rest of the image. This local recomputation is the criterion for the final spatial distribution in the image of the original quantized values.

In the example shown in Fig. 14, the original and filtered images are shown together with their channel histograms. The original image has eight values per channel. For this test, ACE uses a linear scaling in its second phase to not add an additional lightness change, and the slope of  $r(\cdot)$  is set to 5 instead of 20 to not increase the overall contrast.

Observing the histogram shapes in Fig. 14, it can be noticed that while the presented Retinex implementation is mainly a WP approach, ACE has both WP and GW behaviors. In fact, Retinex dequantization can be noticed in the histogram mainly on the right side of dequantized values, while ACE effect can be seen in both darker and lighter directions. The dequantization effect can also be verified in Table 6, where the percentage of used image dynamic is shown.

#### 4.5 Computing Visual Illusions

The two algorithms have been tested on several visual illusions. The results obtained so far confirm that they behave qualitatively like the human visual system.<sup>7,28,34,38,41,42</sup> Here we present a comparison on an image composed by four simultaneous contrast patterns with different background colors.

This configuration and the relative outputs are shown in Fig. 13. Both the computations follow the expected visual appearance qualitatively, changing the gray centers toward the color opposite to the surrounding color.

It is interesting to note that the two algorithms compute an almost equal shift in the hue channel for all four configurations.

The filtering differences are mainly in the saturation and brightness values for both gray patches and backgrounds. In particular, ACE introduces background shading due to its distance-driven local behavior. Alternative distances and inner parameter configurations are under test to relax this effect. In fact, in our opinion, visual illusions are a useful and interesting test bed for parameter tuning of this kind of color equalization algorithm.

#### 4.6 Computational Time

One of the major problems of these algorithms is the heavy computational time. This problem derives from the necessity to perform comparisons for each pixel to all, or a large number of, pixels in the image. On the contrary, the computational space complexity of the algorithms is not heavy, requiring only the memory to keep the original and filtered image.

Regarding the computational time complexity, Retinex with  $k$  paths crossing  $x$  of the  $N$  pixels of the image for each pixel computation, the number of floating point pixel ratios is  $kxN$ . The value of  $x$  can be controlled by tuning

the path's generation parameters, and  $k$  can be set as a parameter, affecting the quality of the result. The basic ACE algorithm has a higher computational cost,  $O(N^2)$ . To reach more efficient computation [e.g.,  $O(N \log N)$ ], several approaches and solutions have been devised to deal with this problem; however, they are not the subject of this work. For more details, refer to Refs. 32, 33, and 43.

## 5 Conclusions

We present a comparison between Retinex and ACE, two unsupervised color equalization algorithms. Their two computational models are described in detail and common points and differences are discussed.

The two algorithms show comparable properties of lightness and color constancy, image dynamic stretching, and data-driven dequantization. The major difference can be noticed in filtering high-key images, where only ACE equalizes the mean lightness because of the absence in Retinex of a GW compensation mechanism.

Other interesting features of both Retinex and ACE are their global and local filtering effect, and their ability to compute visual appearance in illusory visual configurations. In a reported experiment with four simultaneous contrast patterns, these two algorithms have computed the expected visual appearance with different saturation and brightness, but with the same hue. This interesting result suggests the use of visual illusions for parameter tuning of these algorithms.

## References

1. G. Wyszecky and W. S. Stiles, *Color Science: Concepts and Methods, Quantitative Data and Formulas*, John Wiley and Sons, New York (1982).
2. J. Albers, *Interaction of Color*, Yale University Press, New Haven, CT (1975).
3. R. L. DeValois and K. DeValois, *Spatial Vision*, Oxford University Press, New York (1988).
4. E. Land and J. McCann, "Lightness and retinex theory," *J. Opt. Soc. Am.* **61**, 1–11 (1971).
5. D. J. Jobson, Z. Rahman, and G. A. Woodel, "Properties and performance of a center/surround retinex," *IEEE Trans. Image Process.* **6**, 451–462 (1997).
6. K. Barnard and B. Funt, "Investigations into multi-scale retinex," *Proc. Colour Imaging Multimedia '98*, Derby, UK, pp. 9–17 (1998).
7. J. J. McCann, "Lesson learned from mondrians applied to real images and color gamuts," *Proc. IS&T/SID 7th Color Imaging Conf.*, pp. 1–8 (1999).
8. T. J. Cooper, "Modifications to Retinex to relax reset nonlinearity and implement segmentation constraints," *Proc. SPIE* **4662**, 349–357 (2002).
9. H. K. Rising III, "Analysis and generalization of Retinex by recasting the algorithm in wavelets," *Proc. SPIE* **4662**, 419–427 (2002).
10. R. Sobol, "Improving the Retinex algorithm for rendering wide dynamic range photographs," *Proc. SPIE* **4662**, 341–348 (2002).
11. E. H. Land and J. J. McCann, "Method and system for reproduction based on significant visual boundaries of original subject," U.S. Patent No. 3,553,360 (1971).
12. S. Kagen, E. H. Land, L. A. Ferrari, and J. J. McCann, "Image processing system which detects subject by sensing intensity ratios," U.S. Patent No. 3,651,252 (1972).
13. J. Frankle and J. J. McCann, "Method and apparatus of lightness imaging," U.S. Patent No. 4384336 (1983).
14. J. J. McCann, S. McKee, and T. Taylor, "Quantitative studies in retinex theory: A comparison between theoretical predictions and observer responses to color mondrian experiments," *Vision Res.* **16**, 445–458 (1976).
15. J. J. McCann, "Color constancy: Small overall and large local changes," *Proc. SPIE* **1666**, 310–321 (1992).
16. J. J. McCann, "Rules for colour constancy," *Ophthalmic Physiol. Opt.* **12**, 175–177 (1992).

17. A. Moore, J. Allman, and R. Goodman, "A real-time neural system for color constancy," *IEEE Trans. Neural Netw.* **2**, 237–246 (1991).
18. "Retinex at 40—joint special session," *Proc. SPIE* **4662** (2002) (whole volume).
19. H. K. Hartline, H. G. Wagner, and F. Ratcliff, "Inhibition in the eye of limulus," *J. Gen. Physiol.* **39**, 5:651–673 (1956).
20. J. J. McCann, "Local/global mechanisms for color constancy," *Die Farbe* **34**, 275–283 (1987).
21. J. von Kries, "Sources of color science," in *Chromatic Adaptation*, D. L. MacAdam, Ed., pp. 109–119, MIT Press, Cambridge, MA (1976).
22. G. Buchsbaum, "A spatial processor model for object color perception," *J. Franklin Inst.* **310**(1), 1–26 (1980).
23. G. Wald, "The receptors of human color vision," *Science* **145**, 1007–1016 (1964).
24. J. J. McCann, S. P. McKee, and T. H. Taylor, "Quantitative studies in retinex theory—a comparison between theoretical predictions and observer responses to the color mondrian experiments," *Vision Res.* **16**, 445–458 (1976).
25. E. Land, "The retinex theory of color vision," *Sci. Am.* **237**(3), 2–17 (1977).
26. E. Land, "Recent advances in retinex theory and some implications for cortical computations: Color vision and the natural image," *Proc. Natl. Acad. Sci. USA* **80**, 5163–5169 (1983).
27. J. J. McCann, "Color mondrians experiments without adaptation," *AIC Proc.*, Kyoto, Japan, pp. 159–162 (1997).
28. A. Rizzi, C. Gatta, and D. Marini, "Color correction between gray world and white patch," *Proc. SPIE* **4662**, 367–375 (2002).
29. A. C. Hurlbert, "Formal connections between lightness algorithms," *J. Opt. Soc. Am.* **3**, 1684–1693 (1986).
30. S. N. Pattanaik, J. A. Ferwerda, M. D. Fairchild, and D. P. Greenberg, "A multiscale model of adaptation and spatial vision for realistic image display," *Proc. SIGGRAPH98*, Orlando, FL, pp. 287–298 (1998).
31. G. Ciocca, D. Marini, A. Rizzi, R. Schettini, and S. Zuffi, "Retinex preprocessing of uncalibrated images for color based image retrieval," *J. Electron. Imaging* **12**(1), 161–172 (2003).
32. A. Rizzi, C. Gatta, and D. Marini, "A new algorithm for unsupervised global and local color correction," *Pattern Recog. Lett.* **24**(11), 1663–1687 (2003).
33. A. Rizzi, D. Marini, and L. De Carli, "LUT and multilevel Brownian Retinex color correction," *Machine Graphics Vis.* **11**(2/3), 153–168 (2002).
34. D. Marini and A. Rizzi, "A computational approach to color adaptation effects," *Image Vis. Comput.* **18**, 1005–1014 (2000).
35. S. Zeki, *A Vision of the Brain*, Blackwell Scientific, Oxford (1993).
36. T. Cornsweet, *Visual Perception*, Academic Press, New York (1970).
37. D. Marini and A. Rizzi, "A color appearance approach to image database visual retrieval," *Proc. SPIE* **3964**, 186–195 (1999).
38. A. Rizzi, L. Rovati, D. Marini, and F. Docchio, "Unsupervised corrections of unknown chromatic dominants using a Brownian-path-based Retinex algorithm," *J. Electron. Imaging* **12**(3), 431–441 (2003).
39. D. Marini, A. Rizzi, and M. Rossi, "Color constancy measurement for synthetic image generation," *J. Electron. Imaging* **8**(4), 394–403 (1999).
40. A. Rizzi, C. Gatta, and D. Marini, "YACCD: Yet another color constancy database," *Proc. SPIE* **5008**, 24–35 (2003).
41. B. Funt, F. Ciurea, and J. J. McCann, "Defining Retinex in Matlab," *Proc. 8th Color Imag. Conf.*, pp. 112–121, IS&T (2000).
42. D. Marini and A. Rizzi, "A computational approach to color illusion,"

*Proc. ICIAP97 9th Int. Conf. Image Anal. Process.*, Firenze, Italy (1997).

43. A. Rizzi and C. Gatta, "A local linear lut method for increasing the speed of generic image filtering algorithms," Technical report, Univ. of Milano, Polo di Ricerca di Crema, Note de Palo-Ricerca, 43, pp. 1–7, Italy (2002).



vision. His main research topic is the use of color information with particular attention to color adaptation mechanisms.



**Carlo Gatta** received a degree in electronic engineering at University of Brescia, Italy. He is currently a PhD student in computer science at University of Milano, Italy. Since 2001 he has been doing research in the field of digital imaging and vision. His main research topic is the use of color information in computer vision with particular attention to color adaptation mechanisms.



**Daniele Marini** is an associate professor who graduated in physics in 1972. Since 1978, his research at the Department of Information Sciences of the Università di Milano has encompassed several areas of graphics and image processing, with specific reference to visual simulation, realistic visualization, classification, image recognition, and compression. In Italy he pioneered image synthesis with contributions to the foundation of the journal *PIXEL*, and he was one of the founders of the Aicographics Association. In 1982 he created Eidos, the first Italian company specialized in advanced image processing. Since 1997 he has been a member of the National University Council. In 1998, he was appointed supervisor and coordinator of the initiatives on multimedia at Triennale di Milano. He has published more than 140 papers as well as three books. Presently, he is teaching computer graphics and image processing for the graduate programs on informatics at the Università degli Studi di Milano.